


Synthesis and structural characterization of new perovskite phases, $\text{Ba}_2\text{Bi}_{0.572}\text{TeO}_{6\pm\delta}$ and $\text{SrLa}_2\text{NiFeNbO}_9$

Abdelhadi El Hachmi ^{1,2,a)} and Zouhair Sadoune¹

¹Laboratory of Electronic Systems Information Processing Mechanics and Energetics (SETIME), FS Kenitra, Ibn Tofail University, 14000 Kenitra, Morocco

²Laboratory of Radiation-Matter and Instrumentation, FST Settat, Hassan 1st University, 26000 Settat, Morocco

(Received 17 November 2023; accepted 6 May 2024)

$\text{Ba}_2\text{Bi}_{0.572}\text{TeO}_{6\pm\delta}$ and $\text{SrLa}_2\text{NiFeNbO}_9$ ceramics were prepared in polycrystalline form by conventional solid-state reaction techniques in air. The crystal structures of the title compounds were determined at room temperature from X-ray powder diffraction (XRPD) data using the Rietveld method. The $\text{Ba}_2\text{Bi}_{0.572}\text{TeO}_{6\pm\delta}$ structure crystallizes in a triclinic space group $I\bar{1}$ with unit-cell parameters $a = 6.0272(2)$ Å, $b = 6.0367(1)$ Å, $c = 8.5273(3)$ Å, $\alpha = 90.007(7)^\circ$, $\beta = 90.061(2)^\circ$, and $\gamma = 90.015(4)^\circ$. The tilt system of the BiO_6 and TeO_6 octahedra corresponds to the notation $a^-b^-c^-$. The crystal structure of the $\text{SrLa}_2\text{NiFeNbO}_9$ compound adopts an orthorhombic $Pbnm$ space group with lattice parameters $a = 5.6038(5)$ Å, $b = 5.5988(4)$ Å, and $c = 7.9124(6)$ Å. The BO_6 octahedra ($B = \text{Ni/Fe/Nb}$) sharing the corners in 3D. Along the c -axis, the octahedra are connected by O(1) atoms of $(x,y,1/4)$ positions; while in the ab -plane, they are linked by O(2) atoms of (x,y,z) positions. The bond angle of $B\text{--}O1\text{--}B$ is 168.7° and that of $B\text{--}O2\text{--}B$ is 156.3° . The octahedral lattice corresponds to the tilt pattern $a^-a^-c^+$; it indicates that the octahedra tilt out-of-phase along the a,b -axes and in phase along the c -axis.

© The Author(s), 2024. Published by Cambridge University Press on behalf of International Centre for Diffraction Data. This is an Open Access article, distributed under the terms of the Creative Commons Attribution licence (<http://creativecommons.org/licenses/by/4.0/>), which permits unrestricted re-use, distribution and reproduction, provided the original article is properly cited.

[doi:10.1017/S0885715624000289]

Key words: X-ray diffraction, Rietveld method, crystal structure, solid-state reaction, perovskite oxides

I. INTRODUCTION

Among inorganic materials, the ordered double perovskite of the $\text{A}_2\text{BB}'\text{O}_6$ family is one of the most studied by the scientific community due to its wide variety of interesting physical properties, including magnetic, magnetocaloric, ferroelectric, superconducting, photonic, catalytic, and microwave dielectric (Cava and Batlogg, 1989; Fukushima et al., 2011; El Hachmi et al., 2022, 2023; Guo et al., 2022; El Hachmi and Manoun, 2023; Algahtani et al., 2024).

The double perovskite structures $\text{Sr}_2\text{MMoO}_{6-\delta}$ ($M = \text{Fe, Ni, Mg, Mn, Co, Zn}$) have been reported using X-ray powder diffraction (XRPD) to adopt a lower symmetry of triclinic space group $I\bar{1}$ (Vasala et al., 2010). The calculated Goldschmidt tolerance factor (t) has been found between 0.952 ($M = \text{Mn}$) and 0.984 ($M = \text{Ni}$). The triclinic space group $I\bar{1}$ has also been described for the triple perovskite $\text{LaSr}_2\text{Cr}_2\text{SbO}_9$ at room temperature (Hunter et al., 2017); with unit-cell parameters $a = 5.5344$ Å, $b = 5.5562$ Å, $c = 7.8292$ Å, $\alpha = 89.986^\circ$, $\beta = 90.350^\circ$, and $\gamma = 89.926^\circ$. This material has been reported to exhibit a ferrimagnetic state

below 150 K. It has been found that the B -site cations partially occupy the $2f$ (0,1/2,0) and $2g$ (1/2,0,0) Wyckoff sites.

The ordered double perovskite SrLaCuTaO_6 has been reported by West and Davies (2011), who used neutron powder diffraction (NPD) at 323 K as crystallizing in a triclinic space group $P\bar{1}$ (No. 2) with unit-cell parameters $a = 7.801$ Å, $b = 7.813$ Å, $c = 8.399$ Å, $\alpha = 89.67^\circ$, $\beta = 90.32^\circ$, and $\gamma = 90.09^\circ$. Moreover, the tilt system assignment has been given for the $P\bar{1}$ triclinic structure by the notation $a^+b^-c^-$. It has been noted that all atoms occupy $2i$ (x,y,z) Wyckoff sites.

Similar to our tellurium-based compound, it has been reported that the two materials $\text{Ba}_2\text{Bi}_{2/3}\text{TeO}_6$ and $\text{Ba}_3\text{Bi}_2\text{TeO}_9$ (with the same chemical elements and an order of 0.6667:1 and 2:1 on the B -site cations, respectively) have been prepared using the solid-state method at an annealing temperature of 950 °C and investigated by means of NPD at room temperature (Park and Woodward, 2000). The double perovskite $\text{Ba}_2\text{Bi}_{2/3}\text{TeO}_6$ has been described as crystallizing in cubic symmetry with a $Fm\bar{3}m$ space group. It has also been described that the triple perovskite $\text{Ba}_3\text{Bi}_2\text{TeO}_9$ adopts a trigonal structure with a $P\bar{3}c1$ space group.

On the other hand, the simple perovskites $\text{LaNi}_{0.5}\text{Ti}_{0.5}\text{O}_3$ and $\text{LaNi}_{0.45}\text{Co}_{0.05}\text{Ti}_{0.5}\text{O}_3$ have been studied using the Rietveld method (Souza et al., 2021). These two compounds

^{a)} Author to whom correspondence should be addressed. Electronic mail: elhachmi.abdelhadi@gmail.com



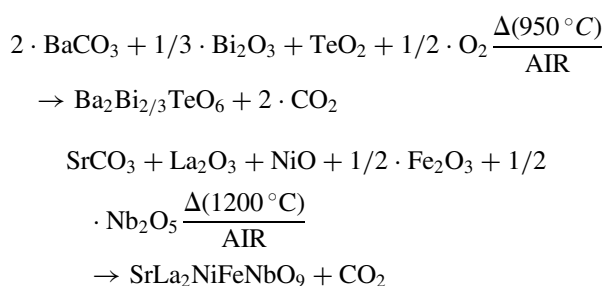
have been described in the orthorhombic structure, with space group $Pbnm$ (No. 62) and Glazer notation $a^-a^-c^+$. The two monoclinic structures $\text{SrLa}_2\text{Ni}_2\text{TeO}_9$ and $\text{Sr}_3\text{NiNb}_2\text{O}_9$ have been characterized by NPD at room temperature and 20 K, respectively; the first compound crystallizes in the $P2_1/n$ space group with lattice parameters $a = 5.6008 \text{ \AA}$, $b = 5.5872 \text{ \AA}$, $c = 7.9018 \text{ \AA}$, and $\beta = 90.021^\circ$ (Sena et al., 2016), and the second structure adopts a $P12_1/c1$ space group with lattice constants $a = 9.7268 \text{ \AA}$, $b = 5.6175 \text{ \AA}$, $c = 16.8704 \text{ \AA}$, and $\beta = 125.024^\circ$ (Lee et al., 2016). Furthermore, the $\text{Sr}_3\text{FeNb}_2\text{O}_9$ compound has been presented as crystallizing in the $P4/mmm$ tetragonal space group (Cha et al., 2014).

In this work, we describe the synthesis procedure and crystal structure determination of the double perovskite oxides $\text{Ba}_2\text{Bi}_{0.572}\text{TeO}_{6\pm\delta}$ and $\text{SrLa}_2\text{NiFeNbO}_9$ from room temperature XRPD using the Rietveld method.

II. EXPERIMENTAL DETAILS

A. Synthesis

Polycrystalline powders of the $\text{Ba}_2\text{Bi}_{0.572}\text{TeO}_{6\pm\delta}$ and $\text{SrLa}_2\text{NiFeNbO}_9$ ceramics were prepared using solid-state reaction route in air, and the raw materials BaCO_3 (99.98%), Bi_2O_3 (99.9%), TeO_2 ($\geq 99\%$), SrCO_3 ($\geq 99.9\%$), La_2O_3 (99.999%), NiO (99%), Nb_2O_5 (99.99%), and Fe_2O_3 ($\geq 96\%$) were used as starting reagents (all received from Sigma-Aldrich). The quantity of each reagent was weighed according to its stoichiometric coefficient to obtain the appropriate metal ratios of the final products, then mixed and ground in an agate mortar to form a homogeneous powder. The resulting mixtures were placed in alumina crucibles, and then increasingly heated in air at different temperature stages with intermittent grinding; these two samples were calcined at 950°C for 12 h and 1200°C for 24 h, respectively. During the heat treatment process, the samples were cooled to room temperature, reground and sintered several times to improve homogeneity. The chemical reactions are:



B. X-ray powder diffraction

Diffraction data of the $\text{Ba}_2\text{Bi}_{0.572}\text{TeO}_{6\pm\delta}$ and $\text{SrLa}_2\text{NiFeNbO}_9$ samples were collected at room temperature on a D2 PHASER diffractometer, with the Bragg-Brentano geometry, using a copper anti-cathode tube as the radiation source ($K_{\alpha 1}$, $K_{\alpha 2}$) of the wavelengths $\lambda(K_{\alpha 1}) = 1.54056 \text{ \AA}$ and $\lambda(K_{\alpha 2}) = 1.54439 \text{ \AA}$ with 30 kV and 10 mA, Soller slits of 0.02 rad on incident and diffracted beams; divergence slit of 0.5° ; anti-scatter slit of 1° ; receiving slit of 0.1 mm ; with sample spinner, and a Lynxeye detector type with a maximum global count rate $> 1\,000\,000\,000 \text{ cps}$. The $\text{Ba}_2\text{Bi}_{0.572}\text{TeO}_{6\pm\delta}$

pattern was scanned in steps of 0.010142° (2θ), between 15 and 105° (2θ) with a fixed-time counting of 2 s per step; while the $\text{SrLa}_2\text{NiFeNbO}_9$ pattern was scanned through steps of 0.020283° (2θ) between 10 and 70° (2θ). The WinPlotr software (Roisnel and Rodríguez-Carvajal, 2001) integrated in the FullProf program (Rodríguez-Carvajal, 1990) was used to determine the crystal structures by means of the Rietveld method (Rietveld, 1969). The peak-shape was described by a pseudo-Voigt function using linear interpolation between set background points with refinable heights.

The following structural and instrumental parameters: scale factor, unit-cell parameters, pseudo-Voigt corrected for asymmetry parameters, FWHM parameters (U , V , and W), preferred orientation, atomic positions, and isotropic thermal factors are included in the refinement of the investigated XRD patterns.

III. RESULTS AND DISCUSSION

A. Crystallite size and microstrain

The crystallite size of these two studied compounds was determined by means of X-ray line broadening using the Scherrer equation and the Williamson-Hall (W-H) method. X-ray peak broadening may be due to crystallite size, microstrain, instrumental profile, temperature factors, and solid solution inhomogeneity. The Scherrer equation can be described by the following expression (Scherrer, 1918):

$$D = \frac{K\lambda}{\beta_{\text{Sch}} \cos \theta} \quad (1)$$

where D is the average crystallite size in (nm), K is the Scherrer constant equal to 0.9, λ is the X-ray wavelength ($\text{Cu } K_{\alpha}$ average = 1.54178 \AA), θ is the Bragg angle of the most intense X-ray diffraction peak and β_{Sch} is the grain size broadening (i.e. full width at half maximum) of the highest peak. Herein, the crystallite size was deduced from the XRD pattern in the strongest peak at $2\theta \approx 29.60^\circ$ for $\text{Ba}_2\text{Bi}_{0.572}\text{TeO}_{6\pm\delta}$ and $2\theta \approx 31.93^\circ$ for $\text{SrLa}_2\text{NiFeNbO}_9$.

According to the Williamson-Hall technique, the strain-induced broadening that results from imperfections and distortions was described by the following equation (Williamson and Hall, 1953):

$$\epsilon = \frac{\beta_s}{4 \tan \theta} \quad (2)$$

where $\epsilon \approx \Delta d/d$ is the upper limit on the lattice distortion, and β_s is the strain broadening in the material. Assuming that the contributions of particle size and strain to the diffraction line broadening are unrelated to each other and that they both have a Cauchy-type profile, the observed peak breadth β_{hkl} can be considered as the sum of the β_s and β_{Sch} widths (El Hachmi and Manoun, 2023):

$$\beta_{hkl} = \beta_s + \beta_{\text{Sch}} \quad (3)$$

and from Eqs (1) and (2), we get

$$\beta_{hkl} \cos \theta = \epsilon(4 \sin \theta) + \frac{K\lambda}{D} \quad (4)$$

TABLE I. Details of Rietveld refinement, crystallite size, and microstrain.

Chemical formula	Ba ₂ Bi _{0.572} TeO _{6±δ}	SrLa ₂ NiFeNbO ₉
M_r (g mol ⁻¹)	617.787	716.870
Temperature (K)	298	298
d_{calc} (g cm ⁻³)	6.614	6.394
Radiation type	Cu K_{α}	Cu K_{α}
Wavelengths (Å)	$\lambda_1 = 1.54056$ ($K_{\alpha 1}$) $\lambda_2 = 1.54439$ ($K_{\alpha 2}$)	$\lambda_1 = 1.54056$ ($K_{\alpha 1}$) $\lambda_2 = 1.54439$ ($K_{\alpha 2}$)
2θ step scan increment (°)	0.010142	0.020283
2θ range (°)	15–105	10–70
Program	FullProf	FullProf
Pseudo-Voigt function	$\eta = 0.32(3)$	$\eta = 0.29(3)$
[PV = $\eta L + (1 - \eta) G$]		
FWHM parameters (U, V, W)	0.001(1), 0.002(2), 0.0055(5)	0.09(2), -0.03(1), 0.011(2)
No. of reflections	748/2	142/2
No. of refined parameter	38	23
Crystal system	Triclinic	Orthorhombic
Space group	$I-1$ (No. 2)	$Pbmm$ (No. 62)
a, b, c (Å)	6.0272(2), 6.0367(1), 8.5273(3)	5.6038(5), 5.5988(4), 7.9124(6)
α, β, γ (°)	90.007(7), 90.061(2), 90.015(4)	90
V (Å ³)	310.26(2)	248.25(4)
Z	2	4
Atom number	4	6
R_B, R_F	3.02, 5.76	4.95, 7.32
R_p, R_{wp}, R_{exp}	7.75, 11.2, 7.59	4.61, 5.99, 4.66
χ^2	2.17	1.65
D_{Sch} (nm)	103.16	79.85
$D_{\text{W-H}}$ (nm)	117.59	150.79
Microstrain ($\epsilon \times 10^{-6}$)	162.6	718.4

By plotting the values of $\beta_{hkl} \cos\theta$ on the y -axis against $4\sin\theta$ on the x -axis, we can determine crystallite size directly from the y -intercept ($K\lambda/D$) and microstrain from the slope (ϵ) of the linear regression line. The values for the crystallite size and microstrain of these two compounds are summarized in Table I. It can be noted that the crystallite size derived by the Williamson-Hall method is larger than that obtained by the Scherrer formula.

B. Crystal structure determination and structure description

At room temperature, the XRD patterns of the two compounds Ba₂Bi_{0.572}TeO_{6±δ} and SrLa₂NiFeNbO₉ are successfully identified by the PDF2 database (Gates-Rector and Blanton, 2019) integrated into the HighScore plus software (Degen et al., 2014) and analyzed using the DICVOL program (Louër and Boulton, 2014) to adopt a single phase related to perovskite structure. Previously, the Ba₂Bi_{2/3}TeO₆ structure was reported to crystallize in cubic symmetry with a $Fm-3m$ space group (Park and Woodward, 2000). The crystal structures of the two studied compounds were determined using the Rietveld analysis method (Rietveld, 1969).

Table I gives the crystal data, data collection, and details of the Rietveld refinements, including lattice parameters, cell volumes, crystal system, space group, and various statistical agreement factors. The values of the reliability factors, R_B , R_F , R_p , R_{wp} , and R_{exp} , and the goodness-of-fit (χ^2), are small and indicate that we have obtained a good quality of the refinements. The quality of the fits is also confirmed by Figures 1 and 2, which provide excellent agreement between the experimental (dots) and theoretical (solid line) patterns. For the Ba₂Bi_{0.572}TeO_{6±δ} compound, the impurity Ba_{0.89}Bi_{8.11}O_{13.05}

(PDF# 00-045-0289) was included in the refinement as a second phase crystallizing in a rhombohedral symmetry $R-3m$ (No. 166) with lattice constants $a = 3.9942$ and $c = 28.4667$ Å. Based on the most intense peaks of both phases, the impurity content is estimated at around 3.5%. The crystal structure presented in Figures 3 and 4 for these two studied compounds were drawn by means of the Vesta software (Momma and Izumi, 2011).

1. Ba₂Bi_{0.572}TeO_{6±δ}

Rietveld refinement analysis reveals that this structure adopts the triclinic symmetry of space group $I-1$ (No. 2) with unit-cell parameters $a = 6.0272(2)$ Å, $b = 6.0367(1)$ Å, $c = 8.5273(3)$ Å, $\alpha = 90.007(7)^\circ$, $\beta = 90.061(2)^\circ$, and $\gamma = 90.015(4)^\circ$. The cell volume is calculated to be 310.26(2) Å³. The number of unit formulas within a cell is $Z = 2$. Reflections from the triclinic structure with space group $I-1$ (No. 2) are correctly indexed on the studied XRD pattern; where the reflection conditions can be described as follows: $hkl \rightarrow h + k + l = 2n$; $0kl \rightarrow k + l = 2n$; $h0l \rightarrow h + l = 2n$; $hk0 \rightarrow h + k = 2n$; $h00 \rightarrow h = 2n$; $0k0 \rightarrow k = 2n$; $00l \rightarrow l = 2n$ (Cockcroft, 1999). The double perovskite Ba₂LaRuO₆ (PDF# 01-085-1103) was used as a starting model for refinement (Battle et al., 1983). It is worth mentioning that the triclinic space group $I-1$ is a non-standard setting of the triclinic space group $P-1$ (No. 2). Fractional atomic coordinates and isotropic thermal parameters are provided in Table II. The structural information indicates that the formal oxidation state of bismuth was oxidized to +3.5 and that of tellurium was oxidized to +6, under synthesis conditions. The site occupancy fraction for bismuth has been refined alone to 0.572(8), and with the constrained occupancies (1 for each Ba, Te, and

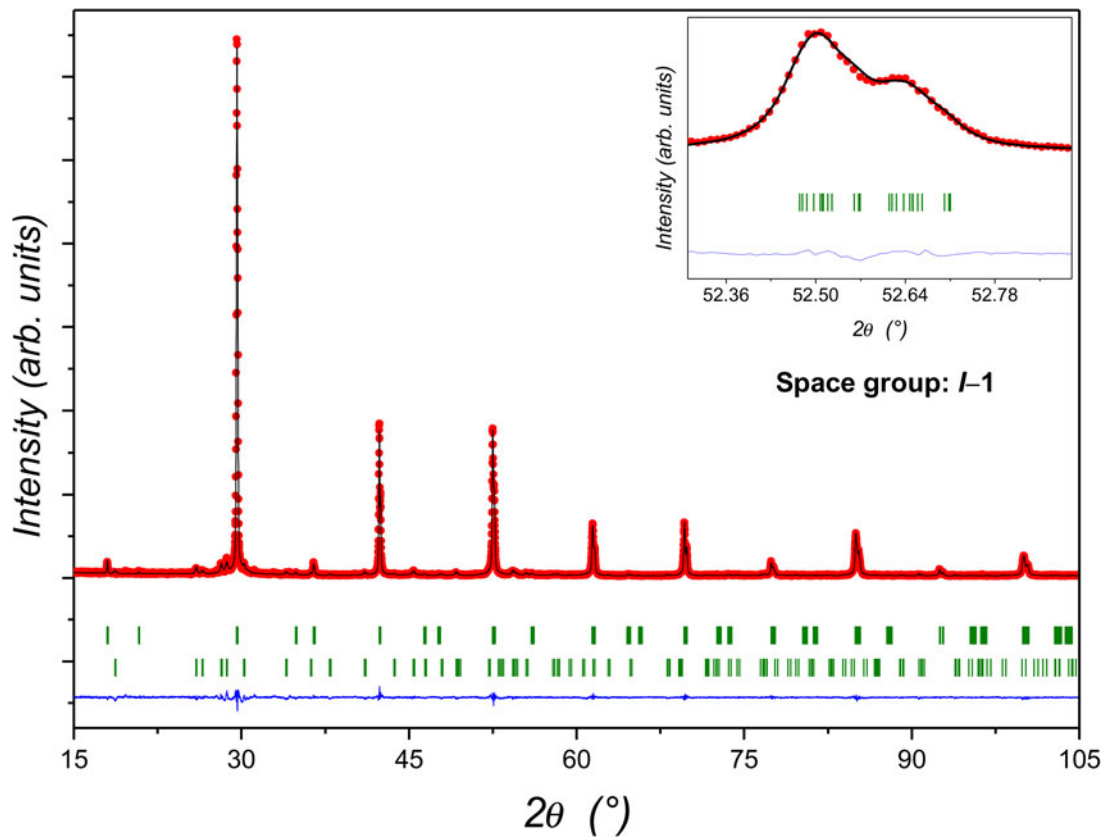


Figure 1. Final Rietveld plot of the triclinic compound $\text{Ba}_2\text{Bi}_{0.572}\text{TeO}_{6\pm\delta}$. The experimental pattern is represented by dots (red) and the calculated pattern is represented by a solid line (black). The vertical (green) marks indicate the Bragg positions of the main phase and the impurity. The lower curve (blue) is the difference diagram.

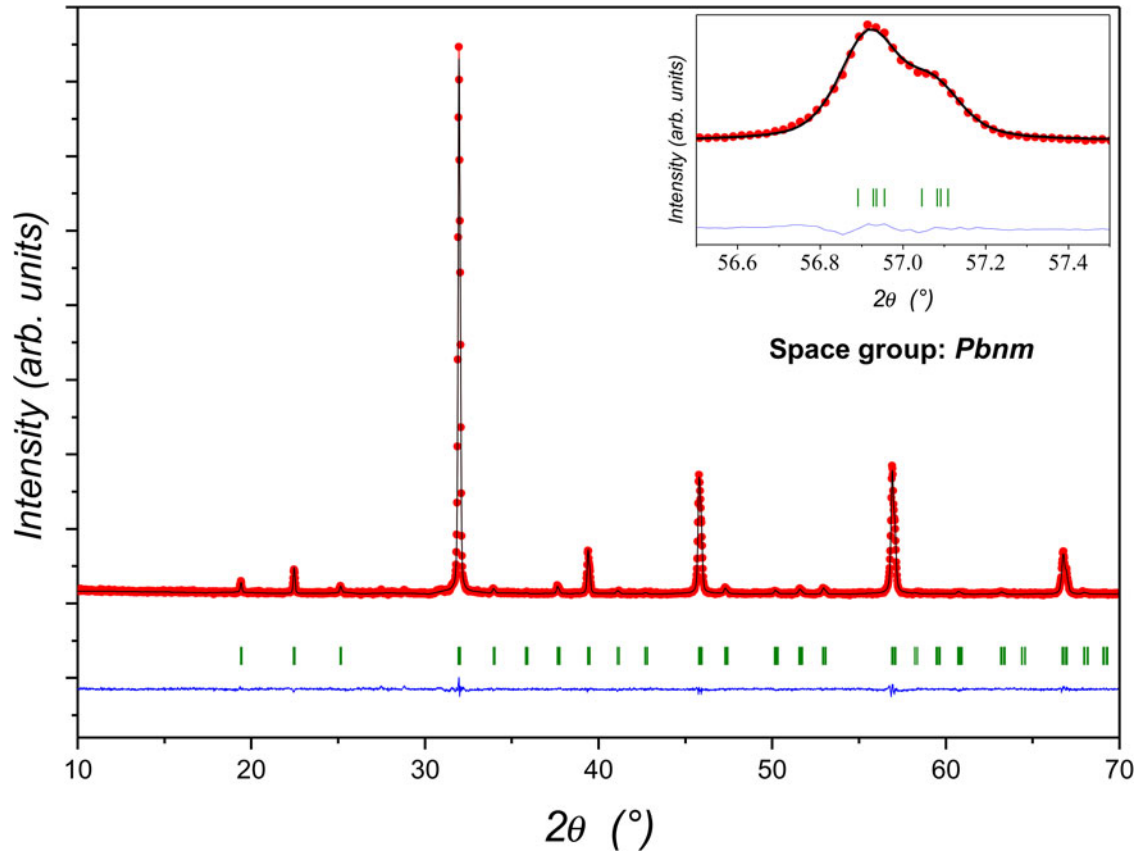


Figure 2. Final Rietveld plot of the orthorhombic compound $\text{SrLa}_2\text{NiFeNbO}_6$. The experimental pattern is symbolized by dots (red) and the calculated pattern is represented by a solid line (black). The vertical (green) marks designate the Bragg positions. The lower curve (blue) is the difference diagram.

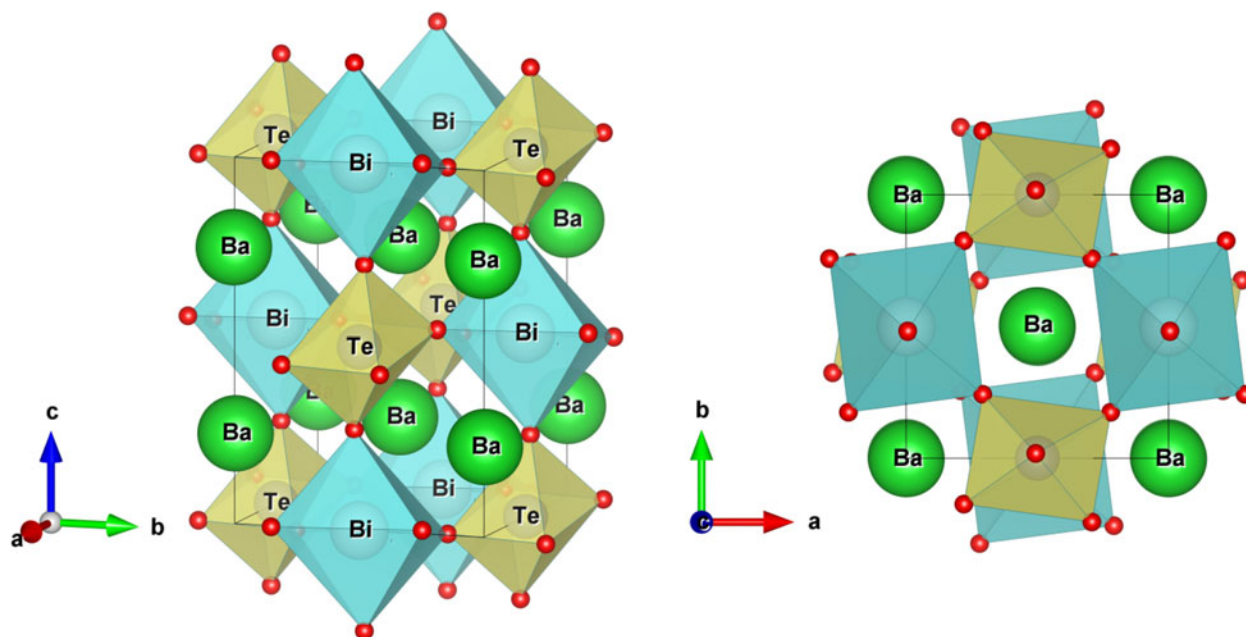


Figure 3. Structural views of the $I-1$ triclinic phase $\text{Ba}_2\text{Bi}_{0.572}\text{TeO}_{6\pm\delta}$. It illustrates octahedra tilt effects in accordance with Glazer's notation $a^-b^-c^-$.

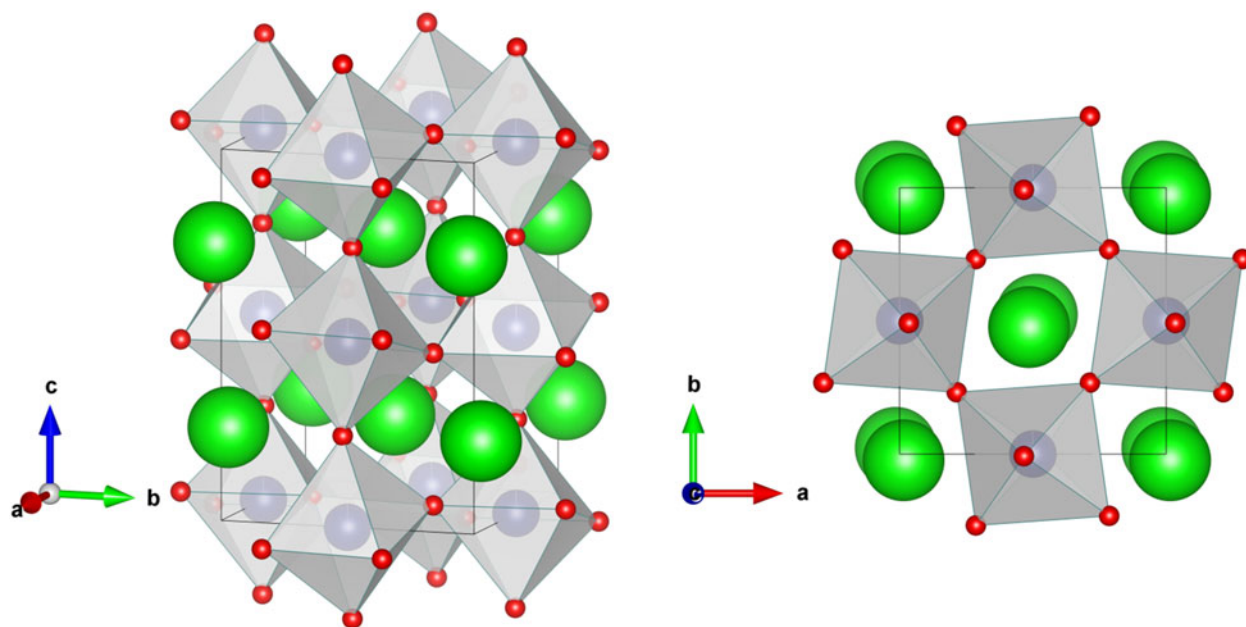


Figure 4. Structural representation of the $Pbnm$ orthorhombic phase $\text{SrLa}_2\text{NiFeNbO}_9$. It shows BO_6 octahedra sharing corners in 3D, as well as octahedral tilting effects in accordance with Glazer notation $a^-a^-c^+$. $\text{Ni}^{2+}/\text{Fe}^{3+}/\text{Nb}^{5+}$ cations are located inside octahedra. $\text{Sr}^{2+}/\text{La}^{3+}$ cations are represented by green spheres.

oxygen), the $\text{Ba}_2\text{Bi}_{0.572}\text{TeO}_{6\pm\delta}$ structure can be considered almost electroneutral. The isotropic displacement parameters B_{iso} (\AA^2) for Ba, Bi, and Te atoms were refined separately, while for oxygen atoms; they were considered equivalent. It can be seen that the isotropic displacement factor B_{iso} of the Bi atom ($1.21(1) \text{\AA}^2$) is greater than that of the Ba, Te, and oxygen atoms. These anomalous isotropic displacement factors can be explained by assuming the presence of a possible positional disorder (either static or dynamic) on the bismuth atoms. The two Bi and Te cations were found to occupy octahedral sites of C_i symmetry at $2f$ ($0, 1/2, 0$) and $2g$ ($1/2, 0, 0$) positions, respectively. The Ba^{2+} and O^{2-} ions were located at $4i$ (x, y, z) positions of C_1 symmetry.

The selected interatomic distances (\AA) and angles (deg.) are given in Table III. The average distances $\langle \text{Ba-O} \rangle$, $\langle \text{Bi-O} \rangle$, and $\langle \text{Te-O} \rangle$ obtained at room temperature after Rietveld refinement of the $\text{Ba}_2\text{Bi}_{0.572}\text{TeO}_{6\pm\delta}$ structure are about the same as those found in other perovskite compounds containing Ba^{2+} , Bi^{3+} , and Te^{6+} cations: $\text{Bi}^{3+}\text{MTe}^{6+}\text{O}_6$ ($M = \text{Cr}^{3+}$, Mn^{3+} , Fe^{3+}) (Kim et al., 2016); $\text{Ba}_2\text{Bi}^{3+}\text{MO}_6$ ($M = \text{Bi}^{5+}$, Sb^{5+}) (Kennedy et al., 2006); and are very close to those calculated from Shannon's effective ionic radii: Ba^{2+} (1.61\AA), Bi^{3+} (1.03\AA), Te^{6+} (0.56\AA), and O^{2-} (1.40\AA) for coordination number 12 and 6 (Shannon, 1976). The Bi and Te cations are surrounded by 6 oxygen ions, and the Ba^{2+} cations are surrounded by 12 oxygen anions.

TABLE II. Atomic coordinates and isotropic temperature factors for triclinic Ba₂Bi_{0.572}TeO_{6±δ} and orthorhombic SrLa₂NiFeNbO₉ phases.

Atom	<i>x</i>	<i>y</i>	<i>z</i>	<i>B</i> _{iso} (Å ²)	Occ.	Wyckoff site	Sym.
Ba ₂ Bi _{0.572} TeO _{6±δ}							
Ba	0.501(2)	0.497(2)	0.254(1)	0.96(8)	1	4 <i>i</i>	1
Bi	0	1/2	0	1.21(1)	0.572(8)	2 <i>f</i>	-1
Te	1/2	0	0	0.28(13)	1	2 <i>g</i>	-1
O(1)	0.292(17)	0.243(16)	0.033(15)	0.5(5)	1	4 <i>i</i>	1
O(2)	0.220(14)	0.825(11)	0.037(9)	0.5(5)	1	4 <i>i</i>	1
O(3)	0.494(13)	0.018(18)	0.225(11)	0.5(5)	1	4 <i>i</i>	1
SrLa ₂ NiFeNbO ₉							
Sr, La	0.9853(6)	0.0234(3)	1/4	1.05(9)	1/3, 2/3	4 <i>c</i>	. <i>m</i> .
Ni, Fe, Nb	1/2	0	0	0.18(7)	1/3, 1/3, 1/3	4 <i>b</i>	-1
O(1)	0.034(3)	0.492(2)	1/4	1.7(3)	1	4 <i>c</i>	. <i>m</i> .
O(2)	0.714(3)	0.268(4)	0.045(2)	1.7(3)	1	8 <i>d</i>	1

TABLE III. Selected interatomic distances (Å) and angles (°).

Ba ₂ Bi _{0.572} TeO _{6±δ}	SrLa ₂ Ni FeNbO ₉	Mean distances	Refs.
1 × Ba–O1	1 × (Sr/La)–O1	2.99(1)	
1 × Ba–O1	1 × (Sr/La)–O1	2.64(1)	Sr/La–O 2.704 Hunter et al. (2017)
1 × Ba–O1	1 × (Sr/La)–O1	2.92(2)	Sr–O 2.774 El Hachmi et al. (2021)
1 × Ba–O1	1 × (Sr/La)–O1	2.70(2)	Ni–O 1.993 Lu et al. (2018)
1 × Ba–O2	2 × (Sr/La)–O2	2.61(2)	Nb–O 2.037 Lu et al. (2018)
1 × Ba–O2	2 × (Sr/La)–O2	3.31(2)	Nb–O 1.990 West and Davies (2011)
1 × Ba–O2	2 × (Sr/La)–O2	2.43(2)	Fe–O 1.963 El Hachmi et al. (2021)
1 × Ba–O2	2 × (Sr/La)–O2	2.91(2)	
1 × Ba–O3			
1 × Ba–O3	<Sr/La–O> _{mean}	2.81	Ba–O 3.006 Park and Woodward (2000)
1 × Ba–O3			Te–O 2.050 El Hachmi et al. (2018)
1 × Ba–O3	2 × B–O1	1.988(2)	Te–O 1.923 Park and Woodward (2000)
<Ba–O> _{mean}	2 × B–O2	1.95(2)	Bi–O 2.380 Kim et al. (2016)
2 × Bi–O1	2 × B–O2	2.09(2)	Bi–O 2.310 Kennedy et al. (2006)
2 × Bi–O2			Bi–O 2.319 Park and Woodward (2000)
2 × Bi–O3	<B–O> _{mean}	2.01	
<Bi–O> _{mean}			
2 × Te–O1	B–O1–B	168.7	
2 × Te–O2	B–O2–B	156.3	
2 × Te–O3			
<Te–O> _{mean}			
Bi–O1–Te	(B = Ni/Fe/Nb)	163	
Bi–O2–Te		151	
Bi–O3–Te		174	

The structural view of the triclinic compound Ba₂Bi_{0.572}TeO_{6±δ} with space group *I*-1 (No. 2) is made up of alternating octahedra sharing corner by means of oxygen atoms, as displayed in Figure 3. Along the *c*-axis, the BiO₆ and TeO₆ octahedra are linked by oxygen atoms O(3) of 4*i* (*x*,*y*,*z*) positions with *x* = 0.494(13), *y* = 0.018(18), and *z* = 0.225(11). Due to the positions occupied by the Bi and Te atoms in sites 2*f* (0,1/2,0) and 2*g* (1/2,0,0), respectively, and by the O(3) oxygen atoms, looking through the *c*-axis, the bond angle Bi–O3–Te is found to be 174°. In the *ab*-plane, the octahedra are connected by the oxygen atoms O(1) and O(2) at sites 4*i* (*x*,*y*,*z*), where the bond angles Bi–O1–Te and Bi–O2–Te are calculated to be 163° and 151°, respectively. The tilting system conforms to Glazer’s notation (*a*⁻*b*⁻*c*⁻); it indicates that the octahedra tilting out-of-phase along the three pseudo-cubic directions [100]_{*p*}, [010]_{*p*}, and [001]_{*p*} with an unequal amplitude, as derived for the ordered double perovskites with an *I*-1 (No. 2) space group of triclinic crystal system (Battle et al., 1983). Each BiO₆ octahedron

consists of six long distances between Bi and O with an average distance of 2.37 Å. While the TeO₆ octahedron consists of six short distances between Te and O, with an average distance of 1.96 Å. The volume of the BiO₆ octahedron is calculated to be 17.204 Å³; and is larger than that observed in the TeO₆ octahedron which is 9.673 Å³.

Since the cell angles determined in the triclinic symmetry are very close to 90°, we attempted to resolve this structure in the *Pbnm* orthorhombic space group, but found that the coordination of the cations on the *A* and *B*-sites increased to 16 instead of 12 for Ba and to 8 instead of 6 for the Bi/Te atoms. For this reason, we concluded that the orthorhombic symmetry is not appropriate for the Ba₂Bi_{0.572}TeO_{6±δ} structure.

2. SrLa₂NiFeNbO₉

This compound was analyzed using the Rietveld refinement method and revealed that its crystal structure adopts an

orthorhombic system of the *Pbnm* (No. 62) space group with lattice parameters $a = 5.6038(5)$ Å, $b = 5.5988(4)$ Å, and $c = 7.9124(6)$ Å. The cell volume was calculated to be $248.25(4)$ Å³. The number of unit formulas contained in a cell is $Z = 4$. It is important to note that the orthorhombic structure with the *Pbnm* (No. 62) space group is properly identified on the XRD pattern as the single perovskite Sr_{0.2}La_{0.8}Ni_{0.8}Te_{0.2}O₃ (PDF# 01-087-0276); where the reflection conditions can be expressed as follows: $0kl \rightarrow k = 2n$; $h0l \rightarrow h + l = 2n$; $h00 \rightarrow h = 2n$; $0k0 \rightarrow k = 2n$; $00l \rightarrow l = 2n$ (Cockcroft, 1999). Impurity phases were not detected in XRD pattern of the as-synthesized sample.

To justify the orthorhombic *Pbnm* model, we also tried to refine the structure in the monoclinic space group *P2₁/n* as was proposed earlier; by introducing the parameters $a = 5.6132$ Å, $b = 5.5973$ Å, $c = 7.9036$ Å, and $\beta = 90.01^\circ$ (PDF# 01-088-0137), and the atomic coordinates of Sr/La at $4i$ (x, y, z) site, Ni/Fe/Nb(1) at $2c$ ($0, 1/2, 0$) site, Ni/Fe/Nb(2) at $2d$ ($1/2, 0, 0$) site, and oxygen atoms at $4i$ (x, y, z) site. This model did not refine well at all stages. For example, the full divergence occurs when refining the FWHM (U, V , and W) and isotropic displacement parameters. It seems that the *P2₁/n* structural model is not very satisfactory.

Atomic positions, isotropic displacement parameters, occupancy, and site symmetry are provided in Table II. The isotropic displacement parameters (B_{iso}) for the oxygen atoms were taken as equivalent, the same for the Ni/Fe/Nb atoms at $4b$ -sites, and Sr/La atoms at $4c$ -sites. It can be noted that the isotropic displacement factor (B_{iso}) of Ni/Fe/Nb atoms ($0.18(7)$ Å²) is quite low compared to that of Sr/La atoms $1.05(9)$ Å², assuming that B -site cations are more

ordered than A -site cations. The fraction of site occupancy for all elements was not refined. Despite some differences in ionic size and valence charge, the three elements Ni²⁺, Fe³⁺, and Nb⁵⁺ have only one crystallographic B -site. As well, the two elements Sr²⁺ and La³⁺ have only one crystallographic A -site in the AA₂B₂B'O₉ triple perovskite structure. The Sr²⁺/La³⁺ cations and O²⁻(1) anions were located at the $4c$ ($x, y, 1/4$) positions of the C_s symmetry. The Ni²⁺, Fe³⁺, and Nb⁵⁺ cations were arranged at the $4b$ ($1/2, 0, 0$) positions with C_i symmetry, and the O²⁻(2) anions were distributed at the $8d$ (x, y, z) sites with C_1 symmetry. The Sr²⁺/La³⁺ cations are surrounded by 12 oxygen ions, and the Ni²⁺/Fe³⁺/Nb⁵⁺ cations are surrounded by 6 oxygen anions. The selected bond lengths (Å) and angles (deg.) obtained from the refined XRD data of the SrLa₂NiFeNbO₉ structure are listed in Table III.

The average distances $\langle \text{Sr/La-O} \rangle$ and $\langle \text{Ni/Fe/Nb-O} \rangle$ obtained at room temperature are comparatively very close to those found in other perovskite compounds containing Sr²⁺, La³⁺, Ni²⁺, Fe³⁺, and Nb⁵⁺ cations; such as SrLa₂Ni₂TeO₉ (Sena et al., 2016), Ba₃NiNb₂O₉ (Lufaso, 2004), and Sr₃Fe_{2+x}Mo_{1-x}O_{9-3x/2} (El Hachmi et al., 2021), and are roughly identical to the distances calculated from Shannon's effective ionic radii; where Sr²⁺ (1.44 Å), La³⁺ (1.36 Å), Ni²⁺ (0.69 Å), Fe³⁺ (0.55 Å), Nb⁵⁺ (0.64 Å), and O²⁻ (1.40 Å) those are for 12- and 6-fold coordination (Shannon, 1976). The structural lattice of the orthorhombic phase (space group *Pbnm*, $Z = 4$) of the triple perovskite SrLa₂NiFeNbO₉ is composed of octahedra with shared corners in three dimensions (3D), as depicted in Figure 4. Along the c -axis, the BO₆ octahedra ($B = \text{Ni/Fe/Nb}$) are linked

TABLE IV. Powder diffraction data of Ba₂Bi_{0.572}TeO_{6±δ} (Cu $K_{\alpha 1}$, $\lambda = 1.54056$ Å).

$2\theta_{\text{obs}}$ (°)	$2\theta_{\text{calc}}$ (°)	$\Delta 2\theta$ (°)	h	k	l	d_{obs} (Å)	d_{calc} (Å)	Δd (Å)	100 I_{obs}/I_0	100 I_{calc}/I_0
18.028	17.988	-0.040	0	-1	1	4.9165	4.92723	0.01073	3	4
	17.990	-0.038	0	1	1		4.92681	0.01030		4
	18.017	-0.011	1	0	1		4.91938	0.00288		2
29.630	29.571	-0.059	0	2	0	3.0124	3.01833	0.00593	100	100
	29.588	-0.042	-1	1	2		3.01665	0.00425		80
	29.590	-0.040	-1	-1	2		3.01644	0.00404		89
	29.609	-0.021	1	-1	2		3.01456	0.00216		91
	29.615	-0.015	1	1	2		3.01397	0.00157		96
	29.619	-0.011	2	0	0		3.01359	0.00119		92
36.480	36.440	-0.040	0	-2	2	2.4609	2.46362	0.00272	3	4
	36.443	-0.037	0	2	2		2.46340	0.00250		2
	36.462	-0.018	-2	0	2		2.46217	0.00127		4
	36.500	0.020	2	0	2		2.45969	0.00121		4
42.378	42.341	-0.037	2	-2	0	2.1311	2.13288	0.00178	28	52
	42.353	-0.025	2	2	0		2.13232	0.00122		56
	42.363	-0.015	0	0	4		2.13183	0.00073		51
52.533	52.475	-0.058	-1	3	2	1.7406	1.74235	0.00175	27	22
	52.479	-0.054	-1	-3	2		1.74223	0.00163		17
	52.486	-0.047	1	-3	2		1.74202	0.00142		19
	52.497	-0.036	1	3	2		1.74168	0.00108		15
	52.507	-0.026	0	-2	4		1.74137	0.00077		17
	52.510	-0.023	-2	0	4		1.74126	0.00066		20
	52.512	-0.021	0	2	4		1.74122	0.00062		21
	52.519	-0.014	-3	1	2		1.74100	0.00040		20
	52.525	-0.008	-3	-1	2		1.74081	0.00021		18
	52.560	0.027	3	-1	2		1.73972	-0.00088		19
	52.567	0.034	2	0	4		1.73951	-0.00109		18
	52.569	0.036	3	1	2		1.73946	-0.00114		18

Continued

TABLE IV. Continued

$2\theta_{\text{obs}}$ (°)	$2\theta_{\text{calc}}$ (°)	$\Delta 2\theta$ (°)	h	k	l	d_{obs} (Å)	d_{calc} (Å)	Δd (Å)	100 I_{obs}/I_0	100 I_{calc}/I_0
61.483	61.381	-0.102	0	4	0	1.5069	1.50916	0.00226	10	15
	61.424	-0.059	-2	-2	4		1.50822	0.00132		16
	61.466	-0.017	2	-2	4		1.50728	0.00038		16
69.688	61.488	0.005	4	0	0	1.3482	1.50679	-0.00011	10	16
	69.607	-0.081	2	-4	0		1.34956	0.00136		9
	69.624	-0.064	2	4	0		1.34927	0.00107		9
	69.630	-0.058	-3	3	2		1.34917	0.00097		7
	69.646	-0.042	-3	-3	2		1.34890	0.00070		8
	69.661	-0.027	-1	-1	6		1.34865	0.00045		8
	69.662	-0.026	-1	1	6		1.34863	0.00043		6
	69.663	-0.025	3	-3	2		1.34861	0.00041		8
	69.682	-0.006	4	-2	0		1.34828	0.00008		8
	69.685	-0.003	3	3	2		1.34824	0.00004		9
	69.695	0.007	1	-1	6		1.34807	-0.00013		7
	69.699	0.011	4	2	0		1.34800	-0.00020		8
77.449	69.700	0.012	1	1	6	1.2313	1.34799	-0.00022	3	9
	77.412	-0.037	0	-4	4		1.23181	0.00051		7
	77.420	-0.029	0	4	4		1.23170	0.00040		7
	77.466	0.017	-4	0	4		1.23108	-0.00022		7
	77.559	0.110	4	0	4		1.22985	-0.00145		7
85.041	84.945	-0.096	-1	5	2	1.1397	1.14075	0.00105	8	4
	84.950	-0.091	-1	-5	2		1.14070	0.00100		5
	84.952	-0.089	1	-5	2		1.14068	0.00098		4
	84.967	-0.074	1	5	2		1.14052	0.00082		5
	84.970	-0.071	-2	4	4		1.14048	0.00078		5
	84.979	-0.062	-2	-4	4		1.14039	0.00069		4
	85.004	-0.037	-1	-3	6		1.14011	0.00041		4
	85.007	-0.034	-1	3	6		1.14008	0.00038		5
	85.008	-0.033	2	-4	4		1.14007	0.00037		4
	85.017	-0.024	-4	2	4		1.13998	0.00028		5
	85.017	-0.024	-3	1	6		1.13997	0.00027		5
	85.020	-0.021	-3	-1	6		1.13994	0.00024		4
	85.029	-0.012	-4	-2	4		1.13985	0.00015		4
	85.032	-0.009	2	4	4		1.13982	0.00012		5
	85.032	-0.009	1	-3	6		1.13981	0.00011		4
	85.047	0.006	1	3	6		1.13965	-0.00005		4
	85.062	0.021	-5	1	2		1.13948	-0.00022		4
	85.071	0.030	-5	-1	2		1.13939	-0.00031		5
	85.103	0.062	4	-2	4		1.13904	-0.00066		4
	85.116	0.075	3	-1	6		1.13890	-0.00080		5
85.118	0.077	5	-1	2	1.13888	-0.00082	5			
85.123	0.082	4	2	4	1.13882	-0.00088	5			
85.125	0.084	3	1	6	1.13880	-0.00090	4			
85.129	0.088	5	1	2	1.13876	-0.00094	5			
92.539	92.488	-0.051	4	-4	0	1.0660	1.06644	0.00044	2	4
	92.519	-0.020	4	4	0		1.06616	0.00016		5
	92.547	0.008	0	0	8		1.06591	-0.00009		4
	92.786	0.247	4	-4	0		1.06644	0.00044		2
	92.817	0.278	4	4	0		1.06616	0.00016		2
	92.845	0.306	0	0	8		1.06591	-0.00009		2
100.033	99.921	-0.112	0	6	0	1.0053	1.00611	0.00081	4	4
	99.954	-0.079	-3	5	2		1.00587	0.00057		4
	99.979	-0.054	-3	-5	2		1.00568	0.00038		3
	99.983	-0.050	3	-5	2		1.00565	0.00035		4
	99.997	-0.036	-3	3	6		1.00555	0.00025		3
	100.006	-0.027	-3	-3	6		1.00548	0.00018		3
	100.018	-0.015	3	5	2		1.00539	0.00009		3
	100.037	0.004	-5	3	2		1.00526	-0.00004		4
	100.039	0.006	-2	0	8		1.00524	-0.00006		4
	100.057	0.024	0	-2	8		1.00511	-0.00019		3
	100.064	0.031	-5	-3	2		1.00506	-0.00024		3
	100.065	0.032	0	2	8		1.00505	-0.00025		4
	100.091	0.058	5	-3	2		1.00486	-0.00044		4
	100.092	0.059	3	-3	6		1.00486	-0.00045		3
	100.119	0.086	3	3	6		1.00466	-0.00064		4
	100.124	0.091	5	3	2		1.00462	-0.00069		3
	100.131	0.098	2	0	8		1.00457	-0.00073		3
	100.136	0.103	6	0	0		1.00453	-0.00077		3

TABLE V. Powder diffraction data of SrLa₂NiFeNbO₉ (Cu K_{α1}, λ = 1.54056 Å).

2θ _{obs} (°)	2θ _{calc} (°)	Δ2θ (°)	<i>h</i>	<i>k</i>	<i>l</i>	<i>d</i> _{obs} (Å)	<i>d</i> _{calc} (Å)	Δ <i>d</i> (Å)	100 <i>I</i> _{obs} / <i>I</i> _o	100 <i>I</i> _{calc} / <i>I</i> _o
19.450	19.394	-0.056	1	0	1	4.5600	4.5731	0.0131	4	2
22.505	22.429	-0.076	1	1	0	3.9475	3.9607	0.0132	6	4
	22.455	-0.050	0	0	2		3.9562	0.0087		3
25.172	25.123	-0.049	1	1	1	3.5350	3.5418	0.0068	3	2
31.998	31.914	-0.084	2	0	0	2.7947	2.8019	0.0072	100	26
	31.943	-0.055	0	2	0		2.7994	0.0047		25
	31.947	-0.051	1	1	2		2.7990	0.0043		100
34.001	33.940	-0.061	0	2	1	2.6346	2.6391	0.0045	2	1
37.684	37.624	-0.060	2	1	1	2.3851	2.3887	0.0036	3	2
	37.643	-0.041	1	2	1		2.3876	0.0025		0
	37.663	-0.021	1	0	3		2.3864	0.0013		0.4
39.441	39.373	-0.068	2	0	2	2.2828	2.2865	0.0037	10	7
	39.398	-0.043	0	2	2		2.2852	0.0024		7
45.850	45.780	-0.070	2	2	0	1.9775	1.9804	0.0029	23	32
	45.835	-0.015	0	0	4		1.9781	0.0006		15
47.357	47.276	-0.081	2	2	1	1.9180	1.9211	0.0031	2	1
	47.314	-0.043	0	2	3		1.9197	0.0017		1
50.201	50.137	-0.064	3	0	1	1.8158	1.8180	0.0022	2	0.1
	50.178	-0.023	2	1	3		1.8166	0.0008		1
	50.194	-0.007	1	2	3		1.8161	0.0003		1
51.671	51.534	-0.137	3	1	0	1.7676	1.7719	0.0043	2	0.3
	51.567	-0.104	2	2	2		1.7709	0.0033		1
	51.574	-0.097	1	3	0		1.7707	0.0031		0.2
	51.605	-0.066	1	1	4		1.7697	0.0021		1
53.021	52.908	-0.113	3	1	1	1.7257	1.7291	0.0034	2	0.4
	52.947	-0.074	1	3	1		1.7279	0.0022		2
56.971	56.891	-0.080	3	1	2	1.6151	1.6171	0.0020	25	20
	56.928	-0.043	1	3	2		1.6162	0.0011		18
	56.936	-0.035	2	0	4		1.6160	0.0009		11
	56.955	-0.016	0	2	4		1.6155	0.0004		11
66.823	66.710	-0.113	4	0	0	1.3989	1.4010	0.0021	9	4
	66.778	-0.045	0	4	0		1.3997	0.0008		4
	66.787	-0.036	2	2	4		1.3995	0.0006		16

by O(1) oxygen atoms of positions (*x*,*y*,1/4); where the bond angle B–O1–B is calculated to be 168.7°. However, in the *ab*-plane, the BO₆ octahedra are connected by O(2) atoms of positions (*x*,*y*,*z*) and the bond angle B–O2–B is found to be 156.3°.

The interatomic distances between Ni/Fe/Nb and O(1) were calculated to be 1.988(2) Å, and between Ni/Fe/Nb and O(2) were found to be 1.95(2) and 2.09(2) Å. The volume of the BO₆ octahedra was calculated to be 10.7127 Å³. The octahedral lattice corresponds to the Glazer tilting system (*a*⁻*a*⁻*c*⁺); it indicates that the octahedra tilt out-of-phase along the two [100]_{*p*} and [010]_{*p*} pseudo-cubic axes with an equal amplitude and in phase along the [001]_{*p*} axis with a different amplitude, as determined for the “orthorhombic” ABO₃ simple perovskites with the *Pbnm* (No. 62) space group (Mitchell et al., 2017). The *I*_o intensities of the XRPD data presented in Tables IV and V are obtained from the calculated intensities of the Rietveld refinement and the observed intensities of all peaks. The values of the *d*-spacings *d*(Å) were calculated for Cu K_{α1} radiation of wavelength 1.54056 Å.

IV. CONCLUSION

The crystals of the Ba₂Bi_{0.572}TeO_{6±δ} and SrLa₂NiFeNbO₉ perovskites were obtained by conventional solid-state reaction techniques. Their structures were determined at room temperature from XRPD data using the Rietveld method. The crystal structure of the Ba₂Bi_{0.572}TeO_{6±δ} phase adopts an *I*-1 (No. 2)

triclinic system with unit-cell parameters *a* = 6.0272(2) Å, *b* = 6.0367(1) Å, *c* = 8.5273(3) Å, α = 90.007(7)°, β = 90.061(2)°, and γ = 90.015(4)°. The Bi and Te cations fully occupy the octahedral sites at positions 2*f* (0,1/2,0) and 2*g* (1/2,0,0), respectively. Ba²⁺ cations and O²⁻ anions are located at 4*i* (*x*,*y*,*z*) sites. The average distance of ⟨Bi–O⟩ is 2.37 Å, and that of ⟨Te–O⟩ is 1.96 Å. The BiO₆ and TeO₆ octahedra share corners via oxygen atoms. The tilt system is given by the notation (*a*⁻*b*⁻*c*⁻); this means that the octahedra tilting out-of-phase along the three pseudo-cubic axes [100]_{*p*}, [010]_{*p*}, and [001]_{*p*} with an unequal amplitude. On the other hand, Rietveld analysis of the crystal SrLa₂NiFeNbO₉ reveals that its structure adopts an orthorhombic space group *Pbnm* (No. 62) with lattice constants *a* = 5.6038(5) Å, *b* = 5.5988(4) Å, and *c* = 7.9124(6) Å. The BO₆ octahedra (*B* = Ni/Fe/Nb) sharing the corners in 3D. Along the *c*-axis, the octahedra are connected by O(1) atoms of (*x*,*y*,1/4) positions; while in the *ab*-plane, they are linked by O(2) atoms of (*x*,*y*,*z*) positions. The bond angle of B–O1–B is 168.7° and that of B–O2–B is 156.3°. The octahedral lattice corresponds to the tilt pattern (*a*⁻*a*⁻*c*⁺); it indicates that the octahedra tilt out-of-phase along the two [100] and [010] axes and in phase along the [001] axis. The three Ni, Fe, and Nb elements have only one crystallographic *B*-site; similarly, the Sr and La elements have only one crystallographic *A*-site in the structure of AA'₂B₂B'O₉ triple perovskite. The Sr²⁺/La³⁺ cations and O²⁻ (1) anions were located at the 4*c* (*x*,*y*,1/4) positions. The Ni²⁺, Fe³⁺, and Nb⁵⁺ cations were situated at the 4*b* (1/2,0,0)

positions, and the O^{2-} (2) anions were distributed at the $8d(x,y,z)$ sites.

V. DEPOSITED DATA

Selected powder patterns from this XRD study have been submitted to ICDD for inclusion in the Powder Diffraction File. The Crystallographic Information Framework (CIF) files containing the results of the Rietveld refinement (including the raw data) were deposited with the ICDD. The data can be requested at pdj@icdd.com.

CONFLICT OF INTEREST

The authors have no conflicts of interest to declare.

REFERENCES

- Algahtani, A., S. Ali, T. Hussain, A. Ali, A. M. Quraishi, V. Tirth, B. S. Abdullaeva, M. Kamran, M. Aslam, and A. Zaman. 2024. "Studies on Structural, Optical and Microwave Dielectric Properties of Double Perovskite $Sr_2Fe_{1-x}Nb_{1-x}O_6$, Ceramics Synthesized by Solid State Route." *Optical Materials* 148: 114822.
- Battle, P. D., J. B. Goodenough, and R. Price. 1983. "The Crystal Structures and Magnetic Properties of Ba_2LaRuO_6 and Ca_2LaRuO_6 ." *Journal of Solid State Chemistry* 46: 234–44.
- Cava, R. J., and B. Batlogg. 1989. "Superconductivity at High Temperatures Without Copper: $Ba_{1-x}K_xBiO_3$." *MRS Bulletin* 14: 49–52.
- Cha, Y. J., J. S. Bae, T. E. Hong, J. H. Yoon, E. H. Chung, E. D. Jeong, H. G. Kim, P. H. Borse, and K. T. Lim. 2014. "Structural, Optical and Visible-Light Photocatalytic Properties of $Sr_3FeNb_2O_9$ Oxide." *Journal of the Korean Physical Society* 65: 520–25.
- Cockcroft, J. 1999. *A Hypertext Book of Crystallographic Space Group Diagrams and Tables*. London, Birkbeck College, University of London. Accessed January 22, 2024. <http://img.chem.ucl.ac.uk/sgp/large/sgp.htm>.
- Degen, T., M. Sadki, E. Bron, U. König, and G. Nénert. 2014. "The HighScore Suite." *Powder Diffraction* 29 (S2): S13–18.
- El Hachmi, A., and B. Manoun. 2023. "Complex Dielectric, Electric Modulus, Impedance, and Optical Conductivity of $Sr_{3-x}Pb_xFe_2TeO_9$ ($x = 1.50, 1.88$ and 2.17)." *International Journal of Materials Research* 114: 100–10.
- El Hachmi, A., Y. Tamraoui, B. Manoun, R. Haloui, M. A. Elaamrani, I. Saadoun, L. Bih, and P. Lazor. 2018. "Synthesis and Rietveld Refinements of New Ceramics $Sr_2CaFe_2WO_9$ and $Sr_2PbFe_2TeO_9$ Perovskites." *Powder Diffraction* 33: 134–40.
- El Hachmi, A., B. Manoun, M. Sajieddine, Y. Tamraoui, and S. El Ouahbi. 2021. "Synthesis, Structural and Optical Properties of Perovskites-Type: $Sr_3Fe_{2+x}Mo_{1-x}O_{9-3x/2}$ ($x = 0.30, 0.45, 0.60, 0.75$ and 1.00)." *Polyhedron* 200: 115133.
- El Hachmi, A., S. El Ouahbi, B. Manoun, and H. Lassri. 2022. "Magnetic, Magnetocaloric Properties and Phenomenological Model of Perovskite Type: $Sr_3Fe_{2+x}Mo_{1-x}O_{9-3x/2}$ ($x = 0.45, 0.60,$ and 1.00)." *Journal of Superconductivity and Novel Magnetism* 35: 1299–306.
- El Hachmi, A., S. Sen, R. Mondal, M. Paul, A. Saha, J. Im, and G. Biswas. 2023. "Structural, Morphological, Magnetic and Optical Properties of Jeanbandyite Prepared by the Co-Precipitation Method." *Materials Today Communications* 34: 105358.
- Fukushima, T., A. Stroppa, S. Picozzia, and J. M. Perez-Matob. 2011. "Large Ferroelectric Polarization in the New Double Perovskite $NaLaMnWO_6$ Induced by Non-Polar Instabilities." *Physical Chemistry Chemical Physics* 13: 12186–90.
- Gates-Rector, S., and T. Blanton. 2019. "The Powder Diffraction File: A Quality Materials Characterization Database." *Powder Diffraction* 34: 352–60.
- Guo, P., M. An, Y. Shu, X. Peng, Y. Han, H. Hu, W. Chen, Y. Zhao, X. Li, and J. Li. 2022. "Nonlinear Photonics Device Based on Double Perovskite Oxide Ba_2LaTaO_6 for Ultrafast Laser Generation." *Optics and Laser Technology* 155: 108334.
- Hunter, E. C., P. D. Battle, R. P. Sena, and J. Hadermann. 2017. "Ferrimagnetism as a Consequence of Cation Ordering in the Perovskite $LaSr_2Cr_2SbO_9$." *Journal of Solid State Chemistry* 248: 96–103.
- Kennedy, B. J., C. J. Howard, K. S. Knight, Z. Zhang, and Q. Zhou. 2006. "Structures and Phase Transitions in the Ordered Double Perovskites $Ba_2Bi^{III}Bi^VO_6$ and $Ba_2Bi^{III}Sb^VO_6$." *Acta Crystallographica Section B: Structural Science* 62: 537–46.
- Kim, S. W., Z. Deng, Z. Fischer, S. H. Lapidus, P. W. Stephens, M. R. Li, and M. Greenblatt. 2016. "Structure and Magnetic Behavior of Layered Honeycomb Tellurates, $BiM(III)TeO_6$ ($M = Cr, Mn, Fe$)." *Inorganic Chemistry* 55: 10229–37.
- Lee, M., E. S. Choi, J. Ma, R. Sinclair, C. D. Cruz, and H. D. Zhou. 2016. "Magnetism and Multiferroicity of an Isosceles Triangular Lattice Antiferromagnet $Sr_3NiNb_2O_9$." *Journal of Physics: Condensed Matter* 28: 476004.
- Louër, D., and A. Boulouf. 2014. "Some Further Considerations in Powder Diffraction Pattern Indexing with the Dichotomy Method." *Powder Diffraction* 29: S7–12.
- Lu, Z., L. Ge, G. Wang, M. Russina, G. Günther, C. R. dela Cruz, R. Sinclair, H. D. Zhou, and J. Ma. 2018. "Lattice Distortion Effects on the Frustrated Spin-1 Triangular-Antiferromagnet $A_3NiNb_2O_9$ ($A = Ba, Sr,$ and Ca)." *Physical Review B* 98: 094412.
- Lufaso, M. W. 2004. "Crystal Structures, Modeling, and Dielectric Property Relationships of 2:1 Ordered $Ba_3MM'2O_9$ ($M = Mg, Ni, Zn; M' = Nb, Ta$) perovskites." *Chemistry of Materials* 16: 2148–56.
- Mitchell, R. H., M. D. Welch, and A. R. Chakhmouradian. 2017. "Nomenclature of the Perovskite Supergroup: A Hierarchical System of Classification Based on Crystal Structure and Composition." *Mineralogical Magazine* 81: 411–61.
- Momma, K., and F. Izumi. 2011. "VESTA 3 for Three-Dimensional Visualization of Crystal, Volumetric and Morphology Data." *Journal of Applied Crystallography* 44: 1272–76.
- Park, J. H., and P. M. Woodward. 2000. "Synthesis, Structure and Optical Properties of Two New Perovskites: $Ba_2Bi_{2/3}TeO_6$ and $Ba_3Bi_2TeO_9$." *International Journal of Inorganic Materials* 2: 153–66.
- Rietveld, H. M. 1969. "A Profile Refinement Method for Nuclear and Magnetic Structures." *Journal of Applied Crystallography* 2: 65–71.
- Rodríguez-Carvajal, J. 1990. "FullProf: A Program for Rietveld Refinement and Pattern Matching Analysis." In *Satellite Meeting on Powder Diffraction of the XV Congress of the IUCr*, 127. Toulouse, France.
- Roisnel, T., and J. Rodríguez-Carvajal. 2001. "WinPLOTR: A Windows Tool for Powder Diffraction Pattern Analysis." *Materials Science Forum* 378: 118–23.
- Scherrer, P. 1918. "Estimation of the Size and Internal Structure of Colloidal Particles by Means of Röntgen." *Nachrichten von der Gesellschaft der Wissenschaften zu Göttingen* 2: 96–100.
- Sena, R. P., J. Hadermann, C. M. Chin, E. C. Hunter, and P. D. Battle. 2016. "Structural Chemistry and Magnetic Properties of the Perovskite $SrLa_2Ni_2TeO_9$." *Journal of Solid State Chemistry* 243: 304–11.
- Shannon, R. D. 1976. "Revised Effective Ionic Radii and Systematic Studies of Interatomic Distances in Halides and Chalcogenides." *Acta Crystallographica Section A: Crystal Physics, Diffraction, Theoretical and General Crystallography* 32: 751–67.
- Souza, M. M., A. Maza, and P. V. Tuza. 2021. "X-ray Powder Diffraction Data of $LaNi_{0.5}Ti_{0.45}Co_{0.05}O_3$, $LaNi_{0.45}Co_{0.05}Ti_{0.5}O_3$, and $LaNi_{0.5}Ti_{0.5}O_3$ Perovskites." *Powder Diffraction* 36: 29–34.
- Vasala, S., M. Lehtimäki, Y. H. Huang, H. Yamauchi, J. B. Goodenough, and M. Karppinen. 2010. "Degree of Order and Redox Balance in B-Site Ordered Double-Perovskite Oxides, $Sr_2MMoO_{6-\delta}$ ($M = Mg, Mn, Fe, Co, Ni, Zn$)." *Journal of Solid State Chemistry* 183: 1007–12.
- West, D. V., and P. K. Davies. 2011. "Triclinic and Monoclinic Structures of $SrLaCuNbO_6$ and $SrLaCuTaO_6$ Double Perovskites." *Journal of Applied Crystallography* 44: 595–602.
- Williamson, G. K., and W. H. Hall. 1953. "X-ray Line Broadening from Filed Aluminium and Wolfram." *Acta Metallurgica* 1: 22–31.